A Nonlinear ultrasonic SHM method for impact damage localisation in composite panels using a sparse array of piezoelectric PZT transducers

Christos Andreades, Gian Piero Malfense Fierro, Michele Meo
Department of Mechanical Engineering, University of Bath, Bath BA2 7AY, UK

Abstract

Structural health monitoring techniques (SHM) for material damage identification have demonstrated higher sensitivity and accuracy when relying on the assessment of nonlinear features exhibited in the material response under ultrasonic wave propagation. In this paper, a novel nonlinear ultrasonic SHM method is introduced for the localisation of impact damage in composite laminates using an array of surface-bonded sensors. Unlike existing algorithms, this method enables quick selection of a suitable signal transmission frequency based on the combined sensor-material response, it does not rely on baseline data or complex measurements of signal arrival time, and it allows identification of malfunctioning sensors to minimise damage localisation errors. The proposed technique is based on the transmission and reception of ultrasonic waves through the inspected panel. Initially, the functionality of the transducers is inspected by comparing the signal amplitude in both directions of sensor-to-sensor paths. Then a planar map of material nonlinearity parameter β is created, and the damage position is defined as the point of highest β amplitude. Experimental tests on three CFRP panels confirmed successful positioning of barely visible impact damage (BVID) within a range of 4-22 mm. Sensor functionality check was demonstrated on one of the composite laminates, and a malfunctioning transducer was detected. The results suggested that the presented method could be considered an improved alternative to existing SHM techniques for localisation of BVID in composite panels.

Keywords: Composite materials, Structural health monitoring, Damage localisation, Nonlinear ultrasound

1 Introduction

Structural health monitoring (SHM) is a general term for the processes aiming at the detection of material defects or damage using various types of sensing systems, in order to assess the condition and performance of engineering structures [1]. Examples of SHM methods include those based on the evaluation of thermal gradients [2-5], Eddy currents [6-8], vibrations [9-11] and acousto-ultrasonic wave propagation [12-16]. Except for civil, automotive and marine applications, SHM is widely used in aerospace industry mainly because of the high percentage of composite materials incorporated into aircraft structures [17]. Layered composite parts, particularly those made from carbon fibre reinforced plastic (CFRP) layers, have a number of advantages over traditional metal parts. They are strong, stiff and lightweight with great fatigue performance and corrosion resistance [17]. On the other hand, composite laminates may exhibit reduction of their mechanical properties at localised areas where damage is present beneath the surface, in the form of delamination or debonding [18]. This type of damage is not always attributed to manufacturing errors such as fibre misalignment, matrix voids or trapped moisture [18]. In fact, it can also occur from in-service impacts with low-velocity objects, leaving shallow surface dents that are hardly detectable under visual inspection [18]. Barely visible impact damage (BVID) can have serious effects on the integrity of the structure, especially if the damage size grows due to operating stresses, vibrations and temperature differentials [19]. Therefore, reliable SHM methods for on-board identification of damage in composite structures such as aircraft wing skins and fuselage panels is of utmost importance. Ultrasonic techniques (linear and nonlinear) are suitable due to the high damage sensitivity and long wave propagation distances they offer, but also because they can be implemented using lightweight piezoelectric transducers permanently attached or embedded into the structure [20].

Over the last years, many research studies focused on the development of ultrasonic SHM methods and algorithms. Some of them were based on phased array techniques [21-27], which utilised compact sensor arrays to guide wave-beams in all directions within the material (similar to a radar), for interaction with possible defects that would result in wave reflection back to the source. This enabled the creation of two-dimensional cross-sectional images of the inspected material. Another category of SHM methods is that of delay-and-sum beamforming [28-34], where the energy of scattered waves was delayed and summed to form images of scatter locations, based on a delay law defined by the geometry of the specific application, as well as the propagation mode and group velocity of the waves. Moreover, other methods applied the concept of time-reversal [35-41]. Briefly, the signals generated from a source were captured in different paths within a sensor network, and the acquired waveforms are then focused on the source by reversing them in time and re-transmitting them backwards through the material. Any change between the two signals of the same path could be attributed to the presence of damage. Furthermore, probabilistic techniques such as the correlation-based algorithms [42, 43], the maximum-likelihood estimation methods [44, 45] and the reconstruction algorithm for probabilistic inspection of damage (RAPID) [46-52], relied on the comparison between the time-of-arrival or energy-of-arrival of signals in the forward and backward directions of each sensor path. Assuming

a change to these signal characterises was due to defect presence, then the probability of damage existence at a certain point was based on the magnitude of signal difference coefficient (SDC).

Although the methods mentioned above were proved capable of identifying and localising damage in composite materials, the majority of them was dependent on the evaluation of linear ultrasonic features [21-42, 44-48, 50, 52]. This may not be suitable for defect detection in the micro-scale, since impedance mismatch is not high enough to cause wave reflection or scattering. On the other hand, ultrasonic techniques relying on the measurement of nonlinear effects exhibited in the material response (e.g. higher harmonics and sub-harmonics) due to interaction of propagating waves with damaged interfaces offer higher sensitivity to micro-flaws [49, 51, 53, 54]. However, most of the aforementioned linear or nonlinear techniques [22-45, 51, 53], required estimation of wave velocity and arrival time, which can be very complex in composite structures. Also, in many of the above studies [23, 28, 30, 33-38, 40, 43-45, 48, 49, 52], there was lack of explanation about the choice of signal transmission frequency, which could be challenging for successful identification of damage. In addition, the effectiveness of most existing algorithms relied on (i) the changes in the acquired signals compared to baseline signals originally recorded at the undamaged state of the structure [22, 28-32, 34, 41, 43-45, 47, 50], and (ii) the assumption that the transducers included in the array were all functional [20-54]. It is very unlikely though for a structure to be subject to future SHM under the same environmental and boundary conditions as the baseline, and also, sensor networks are susceptible to damage (partial or total) due to corrosion, degradation or impacts. These two issues can introduce significant defect positioning errors.

This paper focuses on the development of a novel nonlinear ultrasonic method for impact damage localisation, with the aim of addressing the above challenges. The proposed method is applied through an algorithm, and it is based on the transmission and reception of ultrasonic waves using a circular array of sensors coupled to the surface of the inspected panel. It enables quick determination of an appropriate signal transmission frequency based on the acoustic response of the material and the transducers. In addition, estimation of damage location does not involve complex calculations related to the time-of-flight, velocity or time-reversal of propagating waves, and the accuracy of defect positioning does not rely on the acquisition of baseline signals (i.e. data obtained at the pristine state of the material). Moreover, this technique is capable of detecting faulty sensors, based on the correlation coefficient between the signals in the forward and backward directions of the paths located around the periphery of the senor network (ref. Section 3.1). Defect location is defined as the point (within the inspected area) corresponding to the maximum amplitude of material nonlinearity parameter β (ref. Section 3.2).

2 Nonlinear Parameter Beta

Parameter β is directly related to the effect of the second harmonic generation in the acoustic response of materials. In general, the waves propagating inside a material can interact and excite cracked interfaces and debonded layers [55]. The frictional (rubbing) or out-of-plane (clapping) excitation at the region of damage

can give rise to waves of higher frequency. In particular, these waves have frequencies that are odd and even multiples of the original signal frequency, and thus they can be identified as higher harmonics in the frequency domain of the captured signal [56]. One-dimensional plane waves moving in a single direction (x-direction) inside the material can be expressed by the following second order elastodynamic wave equation

$$\frac{\partial^2 u(x,t)}{\partial t^2} - c^2 \frac{\partial^2 u(x,t)}{\partial x^2} = \beta c^2 \left(\frac{\partial u(x,t)}{\partial x}\right)\left(\frac{\partial^2 u(x,t)}{\partial x^2}\right), \quad (1)$$

where $u(x,t)$ denotes the wave displacement, c represents the wave velocity and β is a pressure-volumetric nonlinear factor in the second order [57]. The second order perturbation solution of equation (1) is

$$u(x,t) = A_1 \sin(kx - \omega t) - A_2 \cos[2(kx - \omega t)], \quad (2)$$

with

$$A_2 = \frac{\beta k^2 A_1^2}{8} x, \quad (3)$$

where A_1 is the amplitude of the waves received at the fundamental harmonic frequency, A_2 is the amplitude of waves received at the second harmonic frequency related to the nonlinear material behaviour, x is the distance of wave propagation, ω is the angular frequency and k is the wave number [58]. Since k is constant, parameter β can be considered

$$\beta \propto \frac{A_2}{{A_1}^2 x}. \quad (4)$$

Assuming A_2 amplitude is higher when the receiving transducer is closer to the damage location, due to lower attenuation of ultrasonic waves, then β is also expected to be higher in the sensor-to-sensor paths near the damage. Hence, a map of β magnitude across the inspected area can be created by calculating the β values in all paths.

3 Damage Localisation Method

As illustrated in Figure 1, damage localisation was performed using a circular array of eight ultrasonic transducers containing piezoelectric lead zirconate titanate (PZT) disks with central frequency of 310 kHz (PI Ceramic PIC255-00004137). The sensors were coupled to the CFRP panels using water-based gel.

3.1 Sensor Functionality Check

In the initial part of the method, sensor functionality is checked to avoid taking into consideration additional ultrasonic nonlinearities arising from malfunctioning transducers instead of the acoustic response of the CFRP material. As shown in Figure 1, the transducers are inspected by assessing the propagation of ultrasonic waves in both directions of each path on the periphery of the inspected region (d_{12}, d_{21}, d_{23}, d_{32}, etc.). The forward and backward directions between two sensors (e.g. sensors S1 and S2) have the same length and fibre orientation. Hence, signals in directions d_{12} and d_{21} must be almost identical if both sensors are operating normally and no damage exists in the path. This can be confirmed by calculating the Pearson product-moment correlation coefficient (r) for the two time signals. This is a numerical measure of the strength (i.e. signal amplitude) and direction of the linear relationship between two variables. The value of r

ranges from −1 to +1, where ±1 indicates the strongest possible agreement and 0 the strongest possible disagreement [59].

At this point it must be noticed that the comparison between the forward and backward signals is a common technique for sensor inspection in literature. However, the way the sensor functionality check was carried out in this SHM method offers some advantages. Firstly, the waves propagating in the short outer paths are expected to have less interaction with possible material defects compared to the paths crossing through the inspected area. Hence, a change in the signal is more likely to indicate a malfunctioning sensor. In addition, each transducer is checked using the signals acquired only in the two paths connecting it to its adjacent sensors (on either side of it), making the process simpler and quicker. In fact, as illustrated in Figure 1, one value of r is obtained for every pair of sensors (r_{12}, r_{23}, etc.). A transducer is considered faulty, only if the two values of r associated with it are both evidently lower than 1. For example, if r_{12}= 0.323, r_{23}= 0.445 and r_{34} to r_{81}= 0.998, then there is probably an issue with S2. However, if r_{12}= 0.997, r_{23}= 0.445 and r_{34} to r_{81}= 0.998, then sensor S2 cannot be regarded faulty since r_{12} is almost equal to 1. This suggests that the effectiveness of sensor functionality check is not affected by the presence of damage in the peripheral paths, and this is another advantage. For composite plates with different material properties and lay-up, the magnitude of r can vary. Therefore, the following calculation is used to determine what magnitude of r is relatively low. At first, the mean and standard deviation (SD) of all r values is calculated. Then the SD is subtracted from the mean, and the obtained value is set as a limit. Next, the mean of r values being greater than the limit is re-calculated, and used as the final limit. Any r values smaller than 95% of the final limit are assumed “low” and a value of 0.5 is assigned to them. The remaining ones are assumed “high” and become equal to 1. By plotting the paths with values of either 0.5 or 1 helps to decide whether a transducer is malfunctioning.

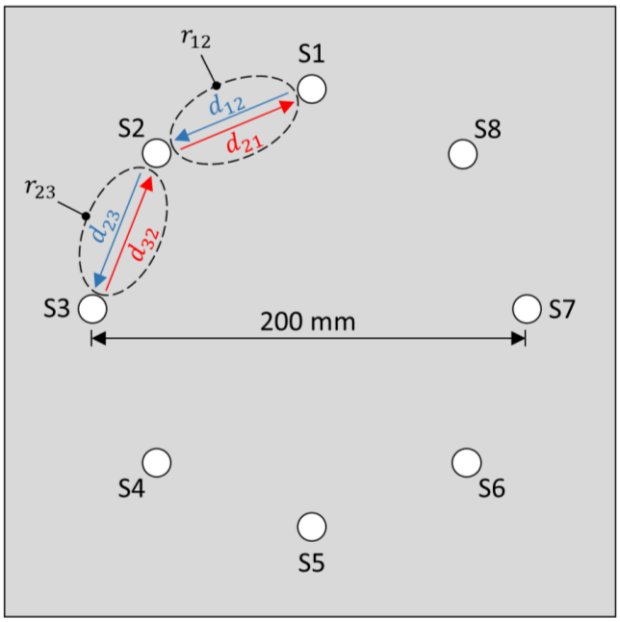

Figure 1: Example of functionality check of sensor S2 based on the correlation coefficients r_{12} and r_{23} of the time signals in directions d_{12}, d_{21} and d_{23}, d_{23} respectively.

3.2 Damage Localisation

The second part of the method enables damage localisation in composite panels by examining the nonlinear ultrasonic response of the material. Every transducer on the array transmits an ultrasonic signal in turn, and the waves propagating inside the material are received by the remaining sensors. The input signal is initially swept from a low frequency (f_L) to a high frequency (f_H), where f_L and f_H are around 200 kHz above and below the central frequency of the transducers. Next, the average of all signals recorded in both directions of the sensor-to-sensor paths is plotted in the frequency spectrum. This allows the identification of the single frequency (f_S) associated with the highest received signal amplitude. At f_S, stronger damage excitation is expected due to higher wave propagation energy. Hence, to achieve damage localisation, the transmission-reception process is performed using driving signals of f_S. The ultrasonic spectrum acquired from each pair of sensors is used to obtain the received signal amplitude (measured as voltage) at f_S and $2f_S$ (i.e. A_{f_s} and A_{2f_s}). According to the theory provided in Section 2, the nonlinear parameter β can be calculated using the following expression

$$\beta_{ij} \propto \frac{A_{2f_s}}{\left(A_{fs}{}^2\right)L_{ij}}, \tag{5}$$

where the subscripts i and j indicate the transmitting and receiving sensors, and L_{ij} is the distance between sensors i and j (i.e. path length).

The path connecting each pair of transducers is then drawn as a flat in-plane ellipse (in x- and y-axes) with an out-of-plane amplitude (z-axis) equal to the corresponding value of β (Figure 2). By adding up the ellipses, a map is created showing the in-plane variation of β magnitude on the composite plate, and the location of maximum β is expected to indicate the position of damage. It must be mentioned that the use of ellipses instead of lines for path representation is common in literature [43, 50, 51, 60]. The main benefit is that depending on the number of sensors used, the minor axis (width) of the ellipses can be adjusted to avoid leaving gaps within the inspected region. This adjustment is required only once for an array of specific size and number of sensors, and it is achieved by trial and error during the drawing of ellipses.

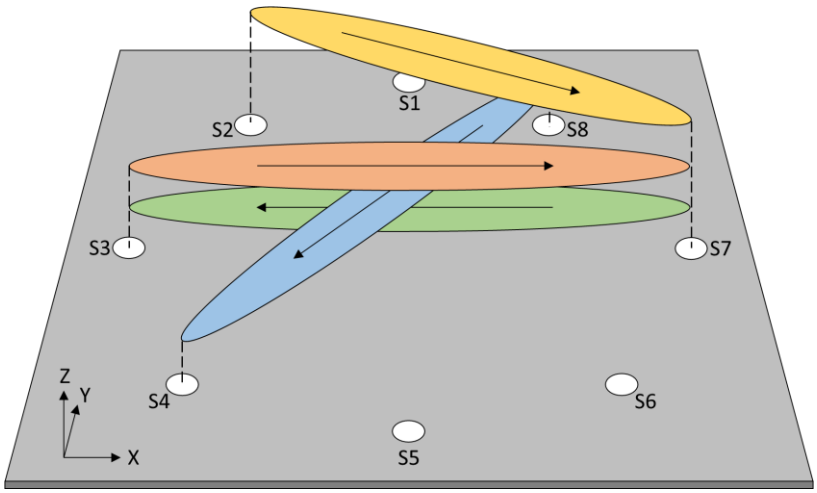

Figure 2: Illustration of nonlinear parameter β amplitude assigned to four sensor-to-sensor paths in the form of ellipses.

4 Experimentation

4.1 CFRP Test Panels

The method explained in the previous section, was experimentally tested on three different CFRP panels of unknown lay-up and prepreg type, with BVID from unknown impact object and energy level. As shown in Figure 3, panels 1 and 2 were flat and rectangular (~13 mm thick), whereas panel 3 was trapezoid (~6 mm thick) and slightly curved in the direction of its long axis.

In all composite laminates, the area around the impact location was examined through C-scanning, to reveal the shape and size of internal delamination. The inspection was performed with a 5 MHz ultrasonic probe made of 128 elements, connected to an imaging system from Diagnostic Sonar Ltd. The results are presented in Figure 4.

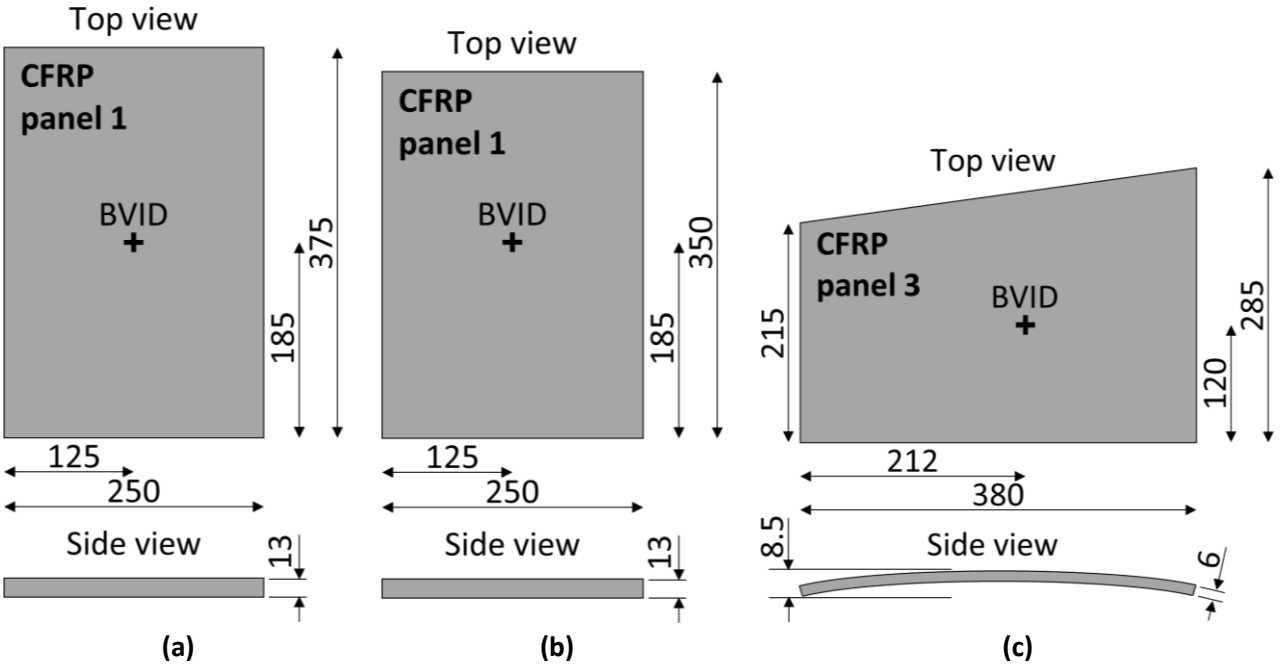

Figure 3: Illustration of CFRP panel 1 (a), 2 (b) and 3 (c) - Dimensions in mm. Not to scale.

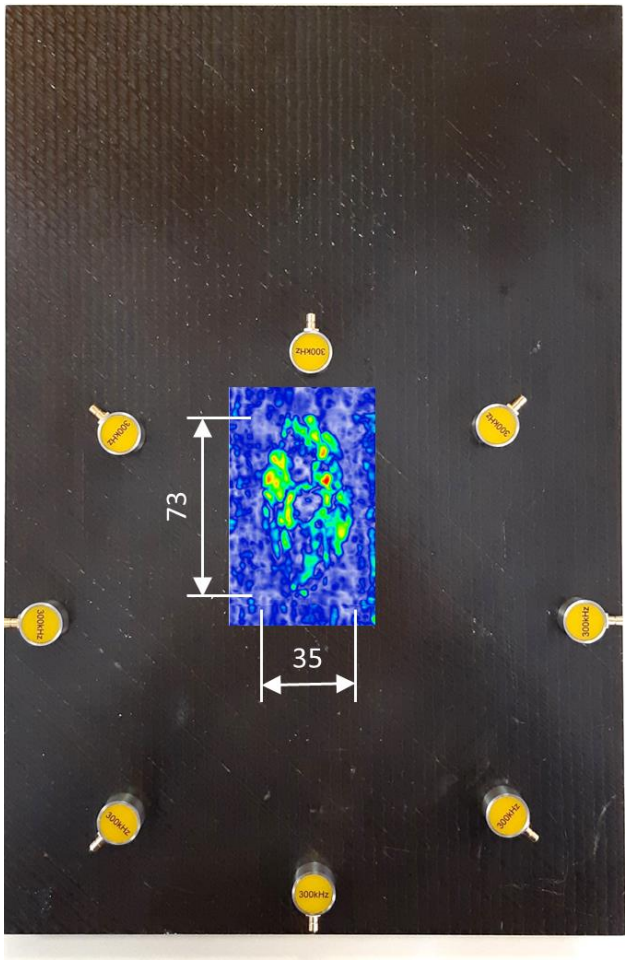

(a)

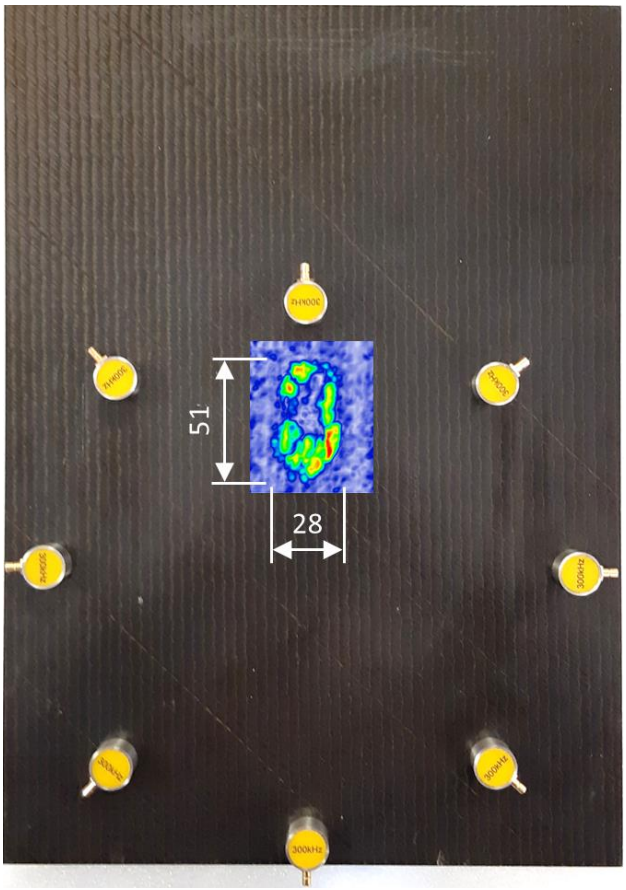

(b)

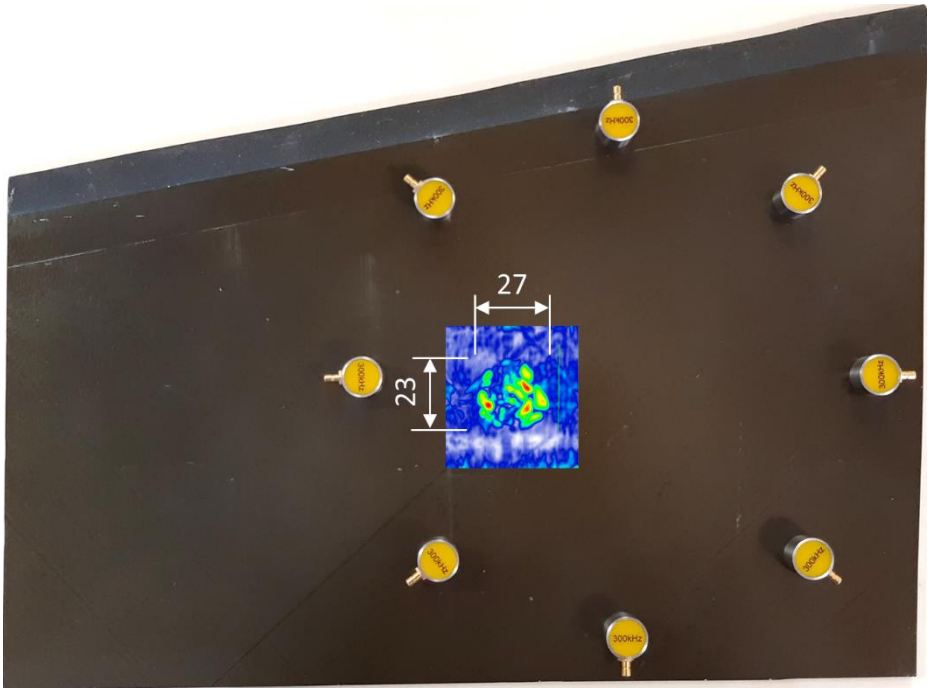

(c)

Figure 4: C-scan around the location of BVID on CFRP panels 1 (a), 2 (b) and 3 (c).

4.2 Ultrasonic Data Acquisition

The set-up illustrated in Figure 5 was used for the acquisition of ultrasonic data in all three CFRP laminates through eight circular piezoelectric PZT transducers (PIC 255 elements) with 310 kHz central frequency. An NI PXI-1033 chassis equipped with a single-channel arbitrary waveform generator module (NI PXI-5421) and an eight-channel signal digitiser module (NI PXI-5105) was controlled by a computer system designed in LabVIEW platform. The input signal voltage was set to 250 V with the use of an amplifier (Falco Systems WMA-300). The process of ultrasonic wave transmission-reception was performed sequentially. At every step, one of the transducers was excited for 10 ms and the propagating waves were captured by the remaining seven sensors over a period of 11 ms at a sampling rate of 6 MHz. This resulted in a total of 56 signals obtained from 28 sensor-to-sensor paths with two directions each.

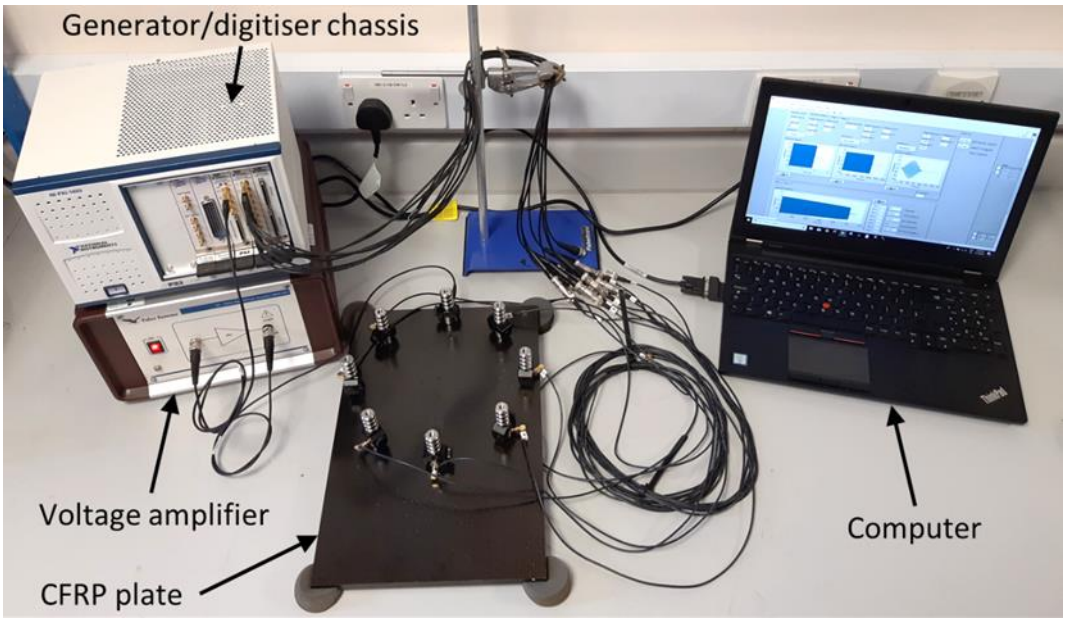

Figure 5: Illustration of the set-up used in the nonlinear ultrasonic experiments.

Prior to performing damage localisation, the ability of the proposed method to inspect the functionality of sensors was demonstrated on CFRP panel 1 following the procedure described in Section 3.1. The input signal frequency was swept from 100 kHz (f_L) to 500 kHz (f_H). Initially, ultrasonic data were recorded using eight fully functional transducers. Then, sensor S6 was replaced with an identical transducer that was partially damaged due to accidental application of high voltage for long period, and data acquisition was repeated. In the latter case, correlation coefficients r_{56} and r_{67} were expected to be evidently lower than the remaining r values, thus they were expected to be assigned with a value of 0.5.

Moving to the damage localisation process, the eight-sensor array was positioned on each CFRP panel as shown in Figure 6. The exact coordinates of the sensors and the damage were listed in Table 1, with the origin taken as the bottom left corner of the panels. Starting from panel 1, the sensor array was placed at two different positions around the BVID (Figure 6a) to confirm that the detected damage location would change

relative to the array. Next, the experiment was carried out on laminate 2 to localise BVID of different size on a CFRP plate with similar thickness. Finally, the method was tested on sample 3, for the detection of BVID position on a thinner CFRP laminate of more complex shape (i.e. curved with unparallel sides).

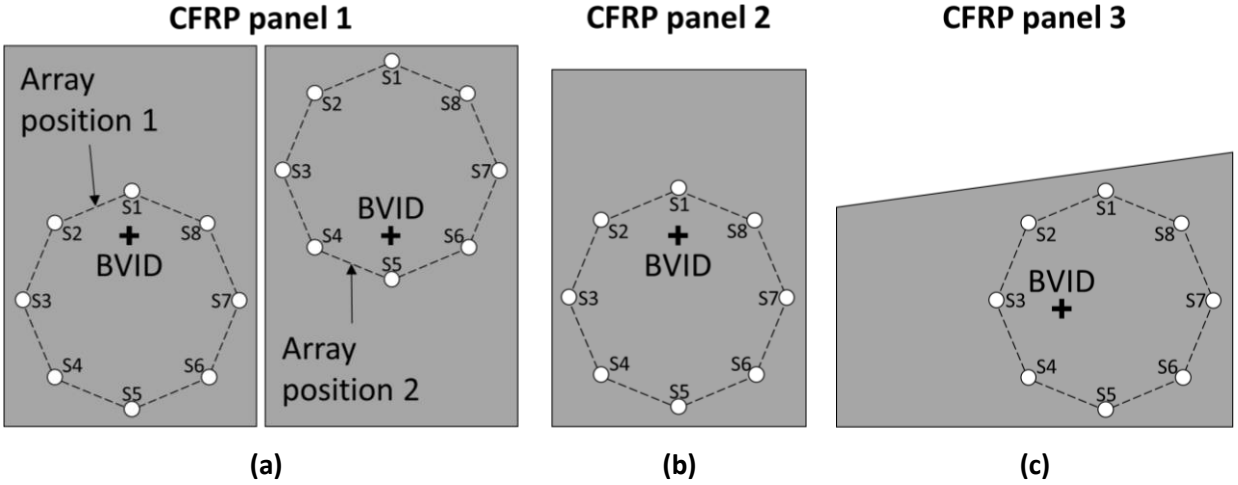

Figure 6: Positioning of sensor array around the location of BVID on CFRP panel 1 (a), 2 (b) and 3 (c).

Table 1: Coordinates of sensors and damage on CFRP panels 1, 2 and 3.

Sensor/Damage ID	Panel 1 - Array 1 x, y (mm)	Panel 1 - Array 2 x, y (mm)	Panel 2 x, y (mm)	Panel 3 x, y (mm)
S1	125, 226	125, 344	125, 222	260, 225
S2	55, 196	55, 314	55, 192	190, 195
S3	25, 126	25, 244	25, 122	160, 125
S4	55, 56	55, 174	55, 52	190, 55
S5	125, 26	125, 144	125, 22	260, 25
S6	195, 56	195, 174	195, 52	330, 55
S7	225, 126	225, 244	225, 122	360, 125
S8	195, 196	195, 314	195, 192	330, 195
Damage	125, 185	125, 185	125, 185	212, 120

The signals of 100-500 kHz sweeps (f_L to f_H) that were previously recorded in all paths during the sensor functionality check, were averaged to obtain the combined frequency response of each CFRP panel. As an example, the average frequency spectrum of CFRP plate 2 was plotted in Figure 7. From this plot, the single frequency f_S corresponding to the highest received signal amplitude (in mV) was identified as 357.9 kHz. According to Section 3.2, the ultrasonic transmission-reception process was performed using input signals of single frequency f_S, and the nonlinear parameter β in each of the 56 paths was calculated from the recorded signal amplitude at f_S and $2f_S$ (ref. equation 5). For example, in the case of panel 2, the spectrum of the signals captured by S1 and S5 under excitation of S3 was plotted in Figure 8. Paths S3-S1 and S3-S5 had the same length and fibre orientation in the material, but only S3-S1 was directly crossing through the damage. As can be seen in Figure 8a, the signal received by S1 had lower amplitude at f_S and higher at $2f_S$, relative to the signal captured by S5 (Figure 8b). Therefore, the β value of path S3-S1 was twice as big as that of S3-S5. In the

same way, the signals captured in all 56 paths of each CFRP panel were used to create the map of β (as explained in Section 3.2) highlighting the location of impact damage.

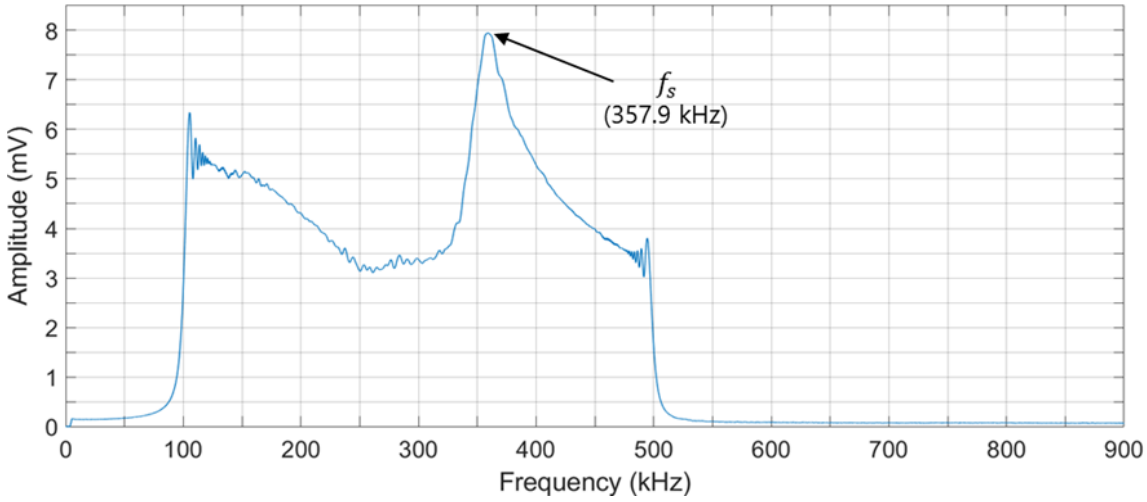

Figure 7: Average plot of the received signals spectrum captured in all paths of CFRP panel 2 under ultrasonic excitation from 100 kHz to 500 kHz.

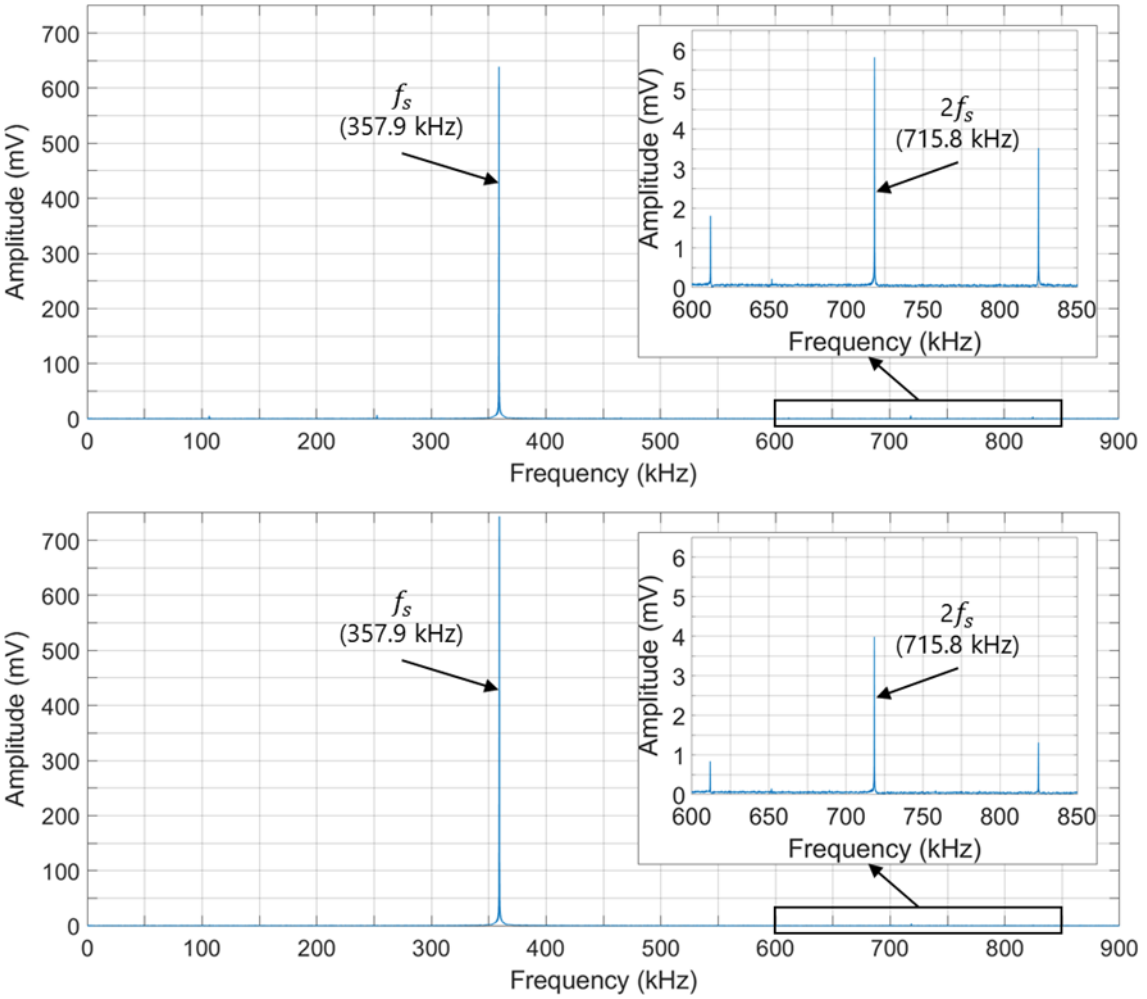

Figure 8: Frequency spectrum of the signal received by (a) sensor S1 and (b) sensor S5 on CFRP panel 2 under ultrasonic excitation of sensor S3 at f_s = 357.9 kHz

5 Results and Discussion

Starting from the sensor functionality check conducted on CFRP panel 1, when all eight transducers were operating normally, the correlation coefficients between the signals in both directions of each sensor-to-sensor path (ie. r_{12} to r_{81}) were all assigned with a value of 1 (see Figure 9a) based on the procedure explained in Section 3.1. However, when a partially damaged transducers was included in the array at position S6, both r_{56} and r_{67} were marked with a value of 0.5 while the remaining r values remained equal to 1 (Figure 9b). This confirmed the capability of the proposed algorithm to detect a malfunctioning sensor.

About the damage localisation results, in CFRP laminate 1 the determined value of f_S related to the highest signal amplitude was found to be 280 kHz for sensor array position 1, and 237.1 kHz for position 2. In panels 2 and 3, f_S was 357.9 kHz and 341.9 kHz respectively. After performing ultrasonic wave transmission at f_S (ref. Section 3.2), the normalised map of nonlinear parameter β on CFRP panel 1 was plotted for each sensor array position (1 and 2), as illustrated in Figure 10a and Figure 10b. The analogous maps of β for panels 2 and 3 were presented in Figure 10c and Figure 10d. In Figure 11, the same maps were plotted after applying a threshold from 0.99 to 1, for better illustration of the peak values of β. According to these maps, the BVID was successfully located in all different cases within an error range of 4 to 22 mm (average of ~12 mm). It must be noted that the localisation error was measured from the estimated damage location to the boundary of BVID. If the error was measured from the centre of impact, the corresponding range would be 23 to 43mm. However, this would not be sensible because stronger acoustic nonlinearities may arise from specific areas (e.g. bigger delamination areas) within the damaged region, and not necessarily from the centre of impact. In fact, the C-scans provided in Figure 4 indicated that the areas of bigger delamination were off-centred, and in most cases, they were close to the estimated damage position.

Finally, it is important to be noticed that in the experiments of this paper the transducers were not placed symmetrically away from the laminate edges, and panel 3 was slightly curved with unparallel sides. This suggested that multi-directional wave reflections of different amplitude had not a significant effect on the accuracy of the presented method.

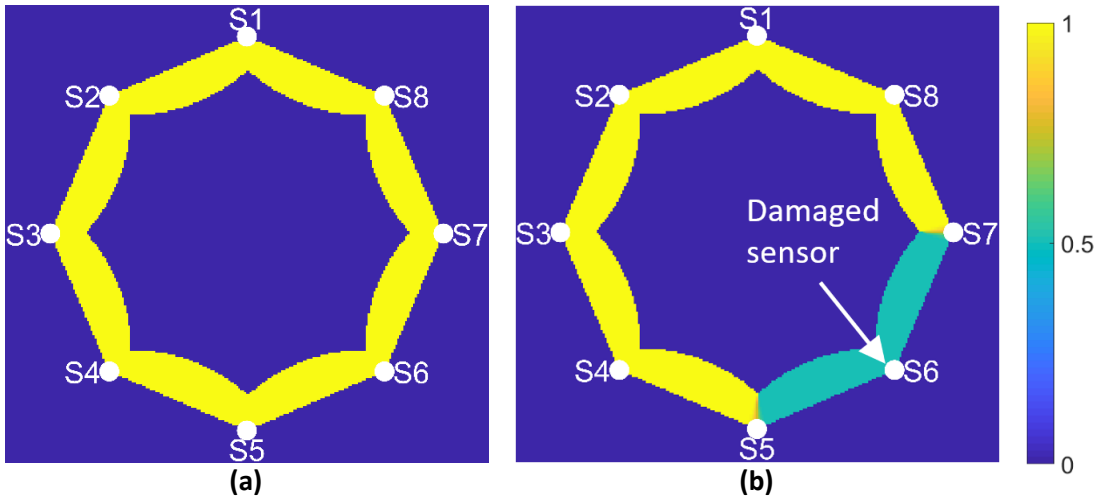

Figure 9: Plot of correlation coefficients between the forward and backward signals in outer sensor-to-sensor paths using eight functional sensors (a) and after replacing S6 with a partially damaged sensor (b).

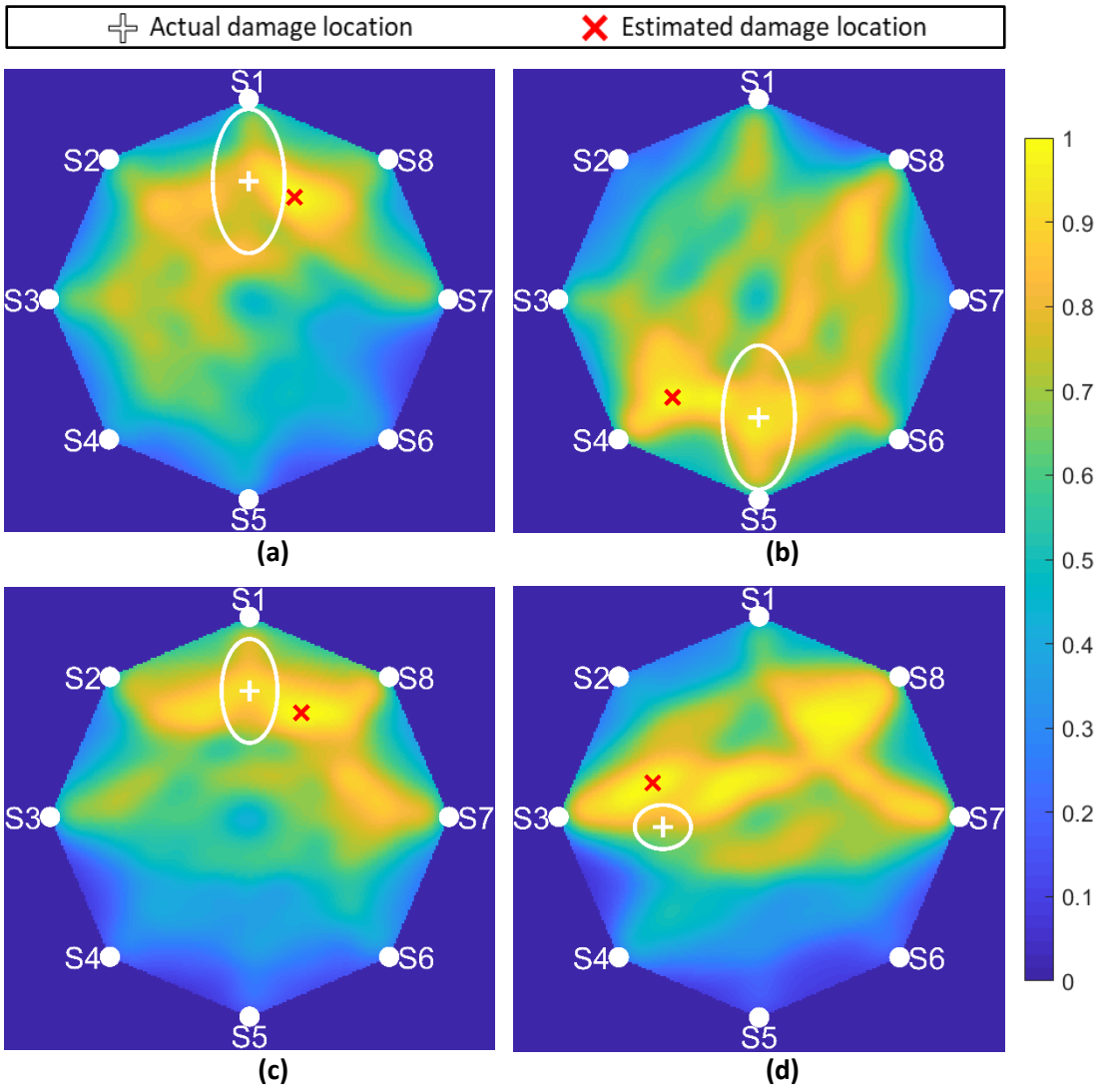

Figure 10: Normalised map of nonlinear parameter β in CFRP panel 1 - array position 1 (a), panel 1 - array position 2 (b), panel 2 (c) and panel 3 (d). The ellipses represent the actual size of internal delamination.

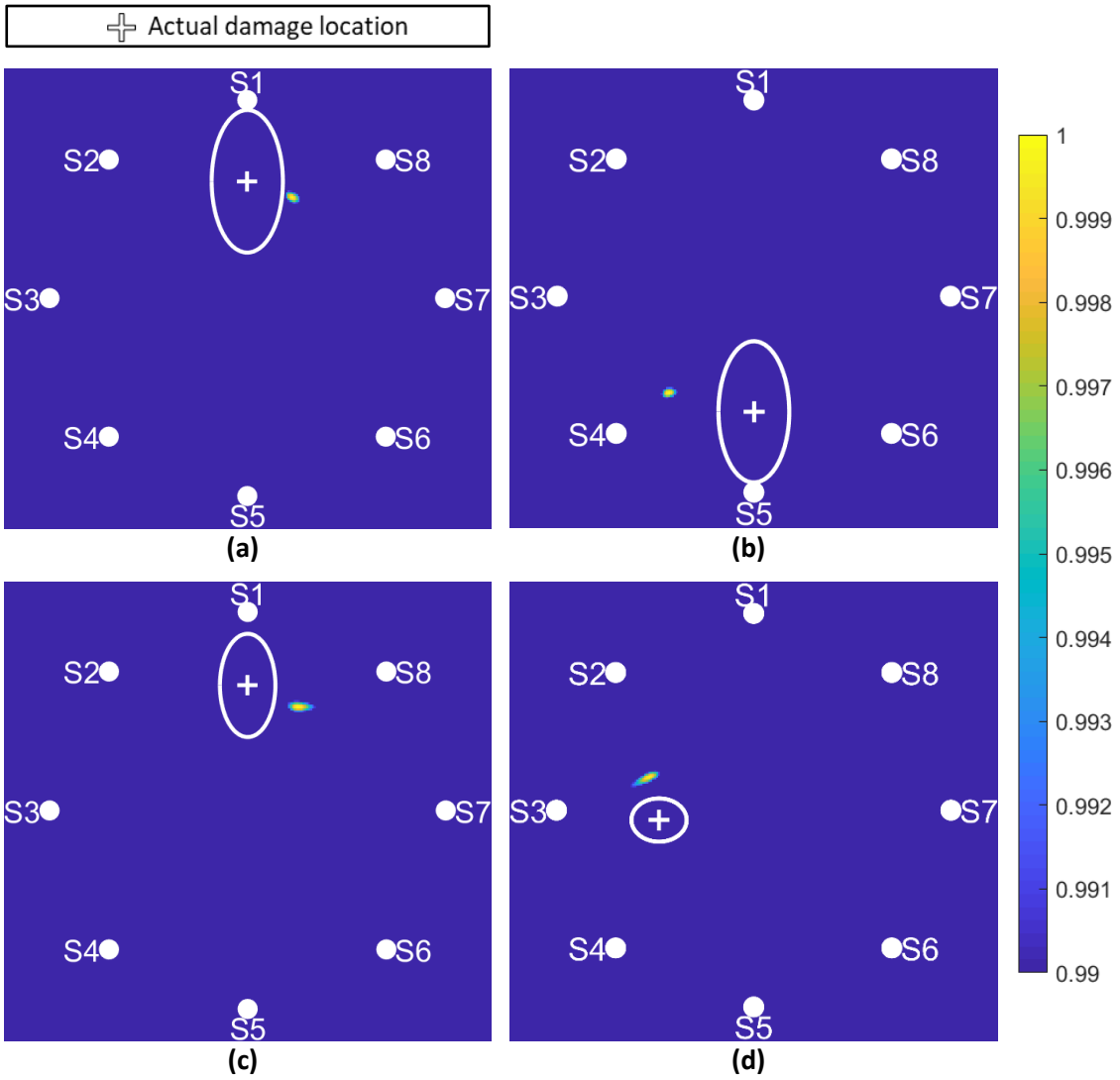

Figure 11: Normalised map with threshold of nonlinear parameter β in CFRP panel 1 - array position 1 (a), panel 1 - array position 2 (b), panel 2 (c) and panel 3 (d). The ellipses represent the actual size of internal delamination.

6 Conclusions

A new method for nonlinear ultrasonic localisation of BVID in composite materials was introduced in this paper. This method involves simple determination of the required signal transmission frequency, there is no need for complex measurements related to the time-of-flight of propagating waves, and the accuracy of damage positioning does not rely on the acquisition of baseline signals (i.e. data obtained at the pristine state of the material). The proposed technique is based on the transmission and reception of ultrasonic waves through the material using a circular array of transducers coupled to the surface of the inspected laminate. As explained in Section 3, this method is capable of checking the functionality of sensors, based on the correlation coefficient between the signals in the forward and backward directions of the paths around the periphery of the senor network. Regarding the detection of damage location, this can be achieved by acquiring ultrasonic signals in sensor-to-sensor paths over a wide range of frequencies (frequency sweep). Once the average of all received signals in the frequency domain is calculated, the frequency associated with the highest received signal amplitude can be determined. Ultrasonic signals of the chosen frequency are then re-transmitted from

every transducer in turn, and the value of nonlinear parameter β in the individual paths is calculated from the signal received by the remaining sensors. By summing up the β values, a map of the material nonlinearity amplitude across the composite panel can be created.

The effectiveness of the presented method was experimentally tested on three CFRP panels of unknown lay-up and prepreg type with different dimensions, shape and size of BVID. In all cases, the position of damage was estimated with an accuracy of 4 to 22 mm, and the detection of a malfunctioning transducer was successfully demonstrated on CFRP laminate 1. Based on the above, it is concluded that the proposed method can be considered an improved alternative to existing techniques for localisation of damage in fibre reinforced composite laminates.

References

1. Yeum, C. M., Sohn, H., Ihn, J. B., & Lim, H. J. (2012). Instantaneous delamination detection in a composite plate using a dual piezoelectric transducer network. *Composite Structures*, 94(12), 3490-3499.
2. Vavilov, V. P., & Burleigh, D. D. (2015). Review of pulsed thermal NDT: Physical principles, theory and data processing. *NDT & E International*, 73(1), 28-52.
3. Chrysafi, A. P., Athanasopoulos, N., & Siakavellas, N. J. (2017). Damage detection on composite materials with active thermography and digital image processing. *International Journal of Thermal Sciences*, 116(1), 242-253.
4. Wang, Z., Tian, G., Meo, M., & Ciampa, F. (2018). Image processing based quantitative damage evaluation in composites with long pulse thermography. *NDT & E International*, 99(1), 93-104.
5. Deane, S., Avdelidis, N. P., Ibarra-Castanedo, C., et al. (2019). Application of NDT thermographic imaging of aerospace structures. *Infrared Physics & Technology*, 97(1), 456-466.
6. Cheng, J., Qiu, J., Xu, X., Ji, H., Takagi, T., & Uchimoto, T. (2016). Research advances in eddy current testing for maintenance of carbon fiber reinforced plastic composites. *International Journal of Applied Electromagnetics and Mechanics*, 51(3), 261-284.
7. Hamill, L., Emerson, J., McGushion, K., & Nutt, S. (2018). Low frequency eddy current testing of insulators and composites. *Journal of Nondestructive Evaluation*, 37(3), 58.
8. Mizukami, K., bin Ibrahim, A. S., Ogi, K., Matvieieva, N., Kharabet, I., Schulze, M., & Heuer, H. (2019). Enhancement of sensitivity to delamination in eddy current testing of carbon fiber composites by varying probe geometry. *Composite Structures*, 226(1), 111227.
9. Dos Santos, F. L. M., Peeters, B., Van der Auweraer, H., Góes, L. C. S., & Desmet, W. (2016). Vibration-based damage detection for a composite helicopter main rotor blade. *Case Studies in Mechanical Systems and Signal Processing*, 3(1), 22-27.
10. Segers, J., Kersemans, M., Hedayatrasa, S., Calderon, J., & Van Paepegem, W. (2018). Towards in-plane local defect resonance for non-destructive testing of polymers and composites. *NDT & E International*, 98(1), 130-133.
11. Samir, K., Brahim, B., Capozucca, R., & Wahab, M. A. (2018). Damage detection in CFRP composite beams based on vibration analysis using proper orthogonal decomposition method with radial basis functions and cuckoo search algorithm. *Composite Structures*, 187(1), 344-353.
12. Staszewski, W. J. (2004). Structural health monitoring using guided ultrasonic waves. In *Advances in Smart Technologies in Structural Engineering* (Vol. 1, p. 117-162). Springer.

13. Jhang, K. Y. (2009). Nonlinear ultrasonic techniques for nondestructive assessment of micro damage in material: a review. *International journal of precision engineering and manufacturing*, 10(1), 123-135.

14. Romhany, G., Czigany, T., & Karger-Kocsis, J. (2017). Failure assessment and evaluation of damage development and crack growth in polymer composites via localization of acoustic emission events: a review. *Polymer Reviews*, 57(3), 397-439.

15. Mitra, M., & Gopalakrishnan, S. (2016). Guided wave based structural health monitoring: A review. *Smart Materials and Structures*, 25(5), 053001.

16. Ono, K. (2018). Review on structural health evaluation with acoustic emission. *Applied Sciences*, 8(6), 958.

17. Ghori, S. W., Siakeng, R., Rasheed, M., Saba, N., & Jawaid, M. (2018). The role of advanced polymer materials in aerospace. In *Sustainable Composites for Aerospace Applications* (Vol.1, p. 19-34). Woodhead Publishing.

18. Abbas, S., Li, F., & Qiu, J. (2018). A review on SHM techniques and current challenges for characteristic investigation of damage in composite material components of aviation industry. *Materials Performance and Characterization*, 7(1), 224-258.

19. Sudevan, D., Prakash, R. V., & Kamaraj, M. (2015). Post-impact fatigue response of CFRP laminates under constant amplitude and programmed FALSTAFF spectrum loading. *Procedia Engineering*, 101(1), 395-403.

20. Wu, Z., Liu, K., Wang, Y., & Zheng, Y. (2015). Validation and evaluation of damage identification using probability-based diagnostic imaging on a stiffened composite panel. *Journal of Intelligent Material Systems and Structures*, 26(16), 2181-2195.

21. Wilcox, P. D. (2003). Omni-directional guided wave transducer arrays for the rapid inspection of large areas of plate structures. *IEEE Transactions on Ultrasonics, Ferroelectrics, and Frequency Control*, 50(6), 699-709.

22. Giurgiutiu, V., & Bao, J. (2004). Embedded-ultrasonics structural radar for in situ structural health monitoring of thin-wall structures. *Structural Health Monitoring*, 3(2), 121-140.

23. Malinowski, P., Wandowski, T., Trendafilova, I., & Ostachowicz, W. (2009). A phased array-based method for damage detection and localization in thin plates. *Structural Health Monitoring*, 8(1), 5-15.

24. Leleux, A., Micheau, P., & Castaings, M. (2013). Long range detection of defects in composite plates using Lamb waves generated and detected by ultrasonic phased array probes. *Journal of Nondestructive Evaluation*, 32(2), 200-214.

25. Liu, Z., Sun, K., Song, G., He, C., & Wu, B. (2016). Damage localization in aluminum plate with compact rectangular phased piezoelectric transducer array. *Mechanical Systems and Signal Processing*, 70(1), 625-636.

26. Kudela, P., Radzienski, M., Ostachowicz, W., & Yang, Z. (2018). Structural Health Monitoring system based on a concept of Lamb wave focusing by the piezoelectric array. *Mechanical Systems and Signal Processing*, 108(1), 21-32.

27. Senyurek, V. Y., Baghalian, A., Tashakori, S., McDaniel, D., & Tansel, I. N. (2018). Localization of multiple defects using the compact phased array (CPA) method. *Journal of Sound and Vibration*, 413(1), 383-394.

28. Michaels, J. E. (2008). Detection, localization and characterization of damage in plates with an in situ array of spatially distributed ultrasonic sensors. *Smart Materials and Structures*, 17(3), 035035.

29. Ihn, J. B., & Chang, F. K. (2008). Pitch-catch active sensing methods in structural health monitoring for aircraft structures. *Structural Health Monitoring*, 7(1), 5-19.

30. Cai, J., Shi, L., Yuan, S., & Shao, Z. (2011). High spatial resolution imaging for structural health monitoring based on virtual time reversal. *Smart Materials and Structures*, 20(5), 055018.

31. Qiu, L., Liu, M., Qing, X., & Yuan, S. (2013). A quantitative multidamage monitoring method for large-scale complex composite. *Structural Health Monitoring*, 12(3), 183-196.

32. Sharif-Khodaei, Z., & Aliabadi, M. H. (2014). Assessment of delay-and-sum algorithms for damage detection in aluminium and composite plates. *Smart Materials and Structures*, 23(7), 075007.

33. Yu, L., & Tian, Z. (2016). Guided wave phased array beamforming and imaging in composite plates. *Ultrasonics*, 68(1), 43-53.

34. Nokhbatolfoghahai, A., Navazi, H. M., & Groves, R. M. (2019). Use of delay and sum for sparse reconstruction improvement for structural health monitoring. *Journal of Intelligent Material Systems and Structures*, 30(18-19), 2919-2931.

35. Fink, M. (1992). Time reversal of ultrasonic fields. I. Basic principles. *IEEE Transactions on Ultrasonics, Ferroelectrics, and Frequency Control*, 39(5), 555-566.

36. Wang, C. H., Rose, J. T., & Chang, F. K. (2004). A synthetic time-reversal imaging method for structural health monitoring. *Smart Materials and Structures*, 13(2), 415-423.

37. Ciampa, F., & Meo, M. (2012). Impact detection in anisotropic materials using a time reversal approach. *Structural Health Monitoring*, 11(1), 43-49.

38. Mustapha, S., Ye, L., Dong, X., & Alamdari, M. M. (2016). Evaluation of barely visible indentation damage (BVID) in CF/EP sandwich composites using guided wave signals. *Mechanical Systems and Signal Processing*, 76(1), 497-517.

39. De Simone, M. E., Andreades, C., Hilmi, A. M., Meo, M., & Ciampa, F. (2019). Proof of concept for a smart composite orbital debris detector. *Acta Astronautica*, 160(1), 499-508.

40. Huang, L., Du, J., Chen, F., & Zeng, L. (2019). An Efficient Time Reversal Method for Lamb Wave-Based Baseline-Free Damage Detection in Composite Laminates. *Applied Sciences*, 9(1), 11.

41. Eremin, A., Glushkov, E., Glushkova, N., & Lammering, R. (2019). Guided wave time-reversal imaging of macroscopic localized inhomogeneities in anisotropic composites. *Structural Health Monitoring*, 18(5-6), 1803-1819.

42. Quaegebeur, N., & Masson, P. (2012). Correlation-based imaging technique using ultrasonic transmit-receive array for non-destructive evaluation. *Ultrasonics*, 52(8), 1056-1064.

43. Memmolo, V., Ricci, F., Boffa, N. D., Maio, L., & Monaco, E. (2016). Structural health monitoring in composites based on probabilistic reconstruction techniques. *Procedia Engineering*, 167(1), 48-55.

44. Flynn, E. B., Todd, M. D., Wilcox, P. D., Drinkwater, B. W., & Croxford, A. J. (2011). Maximum-likelihood estimation of damage location in guided-wave structural health monitoring. *Proceedings of the Royal Society A: Mathematical, Physical and Engineering Sciences*, 467(2133), 2575-2596.

45. Haynes, C., & Todd, M. (2015). Enhanced damage localization for complex structures through statistical modeling and sensor fusion. *Mechanical Systems and Signal Processing*, 54(1), 195-209.

46. Gao, H., Shi, Y., & Rose, J. L. (2005). Guided wave tomography on an aircraft wing with leave in place sensors. In *AIP Conference Proceedings* (Vol. 760, p. 1788-1794). AIP Publishing.

47. Zhao, X., Gao, H., Zhang, G., Ayhan, B., Yan, F., Kwan, C., & Rose, J. L. (2007). Active health monitoring of an aircraft wing with embedded piezoelectric sensor/actuator network: I. Defect detection, localization and growth monitoring. *Smart Materials and Structures*, 16(4), 1208-1217.

48. Yan, F., Royer Jr, R. L., & Rose, J. L. (2010). Ultrasonic guided wave imaging techniques in structural health monitoring. *Journal of intelligent material Systems and Structures*, 21(3), 377-384.

49. Tabatabaeipour, M., Hettler, J., Delrue, S., & Van Den Abeele, K. (2014). Reconstruction algorithm for probabilistic inspection of damage (RAPID) in composites. In *11th European conference on non-destructive testing (ECNDT 2014)*.

50. Keulen, C. J., Yildiz, M., & Suleman, A. (2014). Damage detection of composite plates by Lamb wave ultrasonic tomography with a sparse hexagonal network using damage progression trends. *Shock and Vibration*, 949671.

51. Hettler, J., Tabatabaeipour, M., Delrue, S., & Van Den Abeele, K. (2016). Linear and nonlinear guided wave imaging of impact damage in CFRP using a probabilistic approach. *Materials*, 9(11), 901.

52. Lambinet, F., Sharif Khodaei, Z., & Aliabadi, F. M. (2018). Effectiveness of RAPID and SSM Algorithms on Composite Scarf Repair. In *Key Engineering Materials* (Vol. 774, p. 535-540). Trans Tech Publications Ltd.

53. Boccardi, S., Calla, D. B., Fierro, G. P. M., Ciampa, F., & Meo, M. (2016). Nonlinear damage detection and localization using a time domain approach. In *Nondestructive Characterization and Monitoring of Advanced Materials, Aerospace, and Civil Infrastructure 2016* (Vol. 9804, p. 98040T). International Society for Optics and Photonics.

54. Boccardi, S., Calla, D. B., Ciampa, F., & Meo, M. (2018). Nonlinear elastic multi-path reciprocal method for damage localisation in composite materials. *Ultrasonics*, 82(1), 239-245.

55. Soleimanpour, R., Ng, C. T., & Wang, C. H. (2017). Higher harmonic generation of guided waves at delaminations in laminated composite beams. *Structural Health Monitoring*, 16(4), 400-417.

56. Ciampa, F., Pickering, S. G., Scarselli, G., & Meo, M. (2017). Nonlinear imaging of damage in composite structures using sparse ultrasonic sensor arrays. *Structural Control and Health Monitoring*, 24(5), 1911.

57. Zagrai, A., Donskoy, D., Chudnovsky, A., & Golovin, E. (2008). Micro-and macroscale damage detection using the nonlinear acoustic vibro-modulation technique. *Research in Nondestructive Evaluation*, 19(2), 104-128.

58. Amura, M., Meo, M., & Amerini, F. (2011). Baseline-free estimation of residual fatigue life using a third order acoustic nonlinear parameter. *The Journal of the Acoustical Society of America*, 130(4), 1829-1837.

59. Taylor, J. R. (1997). *An Introduction to Error Analysis: The Study of Uncertainties in Physical Measurements* (Vol. 1, p. 217). 2nd ed. Sausalito: University Science Books.

60. Zhao Zhao, X., Royer, R. L., Owens, S. E., & Rose, J. L. (2011). Ultrasonic Lamb wave tomography in structural health monitoring. *Smart Materials and Structures*, 20(10), 105002.